ACADEMIC PRESS

Available online at www.sciencedirect.com
SCIENCE DIRECT®

Journal of Solid State Chemistry 170 (2003) 339–350

JOURNAL OF SOLID STATE CHEMISTRY

http://elsevier.com/locate/jssc

Structural and Magnetic Chemistry of $NdBaCo_2O_{5+\delta}$

J.C. Burley,* J.F. Mitchell, S. Short, D. Miller, and Y. Tang

Materials Science Division, Argonne National Laboratory, 9700 South Cass Avenue, Argonne, IL 60439, USA

Received 29 July 2002; received in revised form 25 September 2002; accepted 3 October 2002

Abstract

The crystallographic and magnetic structures of the oxygen-deficient perovskites $NdBaCo_2O_{5+\delta}$ ($\delta = 0, 0.38, 0.5, 0.69$) have been studied as a function of temperature by neutron powder diffraction. Long-range G-type antiferromagnetic order is realized for all samples apart from that with $\delta = 0.5$. The lack of magnetic order for $\delta = 0.5$ can be understood on the basis of a crystal-field-induced spin-state ordering between low-spin and high-spin Co^{3+}. Contrary to studies of similar materials with smaller lanthanides, the $\delta = 0$ material exhibits no evidence of long-range charge ordering. No evidence of a spin-state transition as observed in $YBaCo_2O_5$ is found for any of our samples.

1. Introduction

Cobalt-based perovskites have been the subject of a number of studies in recent years. In addition to the spin, charge and orbital degrees of freedom found in the manganite perovskites, the cobaltates are expected to exhibit a degree of freedom in the electronic configuration of the cobalt ion. For example, $LaCoO_3$ (Co^{3+}) is said to undergo two transitions on warming, from a low-spin (LS) t_{2g}^6 non-magnetic ground state at low temperatures, to states which remain controversial, but likely include contributions from the intermediate-spin (IS) $t_{2g}^5e_g^1$ configuration and the high-spin (HS) $t_{2g}^4e_g^2$ configuration [1–6]. Crystal-field effects are expected to favor the LS state, covalency the IS (via a mixing in of the $|d^7\underline{L}\rangle$), and Hund-like exchange the HS state [3]. For example, low-temperature neutron diffraction studies have shown that CoF_3 (ReO_3 structure type) exhibits an ordered magnetic moment of 4.4 μ_B per Co^{3+} ion, indicative of a high-spin $t_{2g}^4e_g^2$ configuration, whereas in Co_3O_4 (spinel structure type) it is found that the octahedral Co^{3+} does not possess an ordered magnetic moment at base temperature, indicating a low-spin $t_{2g}^6e_g^0$ configuration [7,8]. This is taken to be due to the reduced crystal field at the Co^{3+} site. Of the possible Co^{3+} spin-configurations, the IS state is expected to be Jahn–Teller active due to the quarter-filled e_g manifold; however, no crystallographic evidence of such a distortion has been reported to date in $LaCoO_3$. This is likely in part due to the rhombohedral $R\bar{3}c$ structure of $LaCoO_3$, in which long-range Jahn–Teller distortions cannot be coherent with the crystallographic space group operators. Lower symmetry derivatives of $LaCoO_3$, therefore, may provide opportunities not available in the parent material for structural studies of any spin-state transitions. Here we report the results of our preliminary neutron powder diffraction studies on the layered, oxide deficient $NdBaCo_2O_{5+\delta}$ system. Our goal in this investigation has been to undertake a survey of the structural and magnetic chemistry of $NdBaCo_2O_{5+\delta}$ as a function of oxygen vacancy concentration, with the aim of identifying broad trends, as well as areas important for more thorough study.

The crystal structure adopted by $LnBaCo_2O_{5+\delta}$ Ln = lanthanide (Fig. 1) has been reported to be either tetragonal $P4/mmm$ ($a_p \times a_p \times 2a_p$), orthorhombic Pmmm ($a_p \times 2a_p \times 2a_p$ or $a_p \times a_p \times 2a_p$), or orthorhombic Pmmb ($a_p \times 2a_p \times 2a_p$). Here a_p refers to the basic cubic perovskite cell parameters (ca. 3.9 Å). The doubling in c is due to ordering of Ln and Ba into layers perpendicular to z. The cell doubling in b, and the transition from tetragonal to orthorhombic, have been suggested to arise from an ordering of the oxide ion vacancies into channels at a value of $\delta = 0.5$ [9–11]. For values of $\delta = 0$, long-range antiferromagnetic ordering at $T \sim 340$ K, and long-range charge ordering at $T \approx 210$ K were found for Ln = Gd, Ho, Dy in a neutron

*Corresponding author. Fax: +1-630-252-7777.
E-mail address: burley@anl.gov (J.C. Burley).

0022-4596/03/$ - see front matter © 2002 Elsevier Science (USA). All rights reserved.
doi:10.1016/S0022-4596(02)00101-9

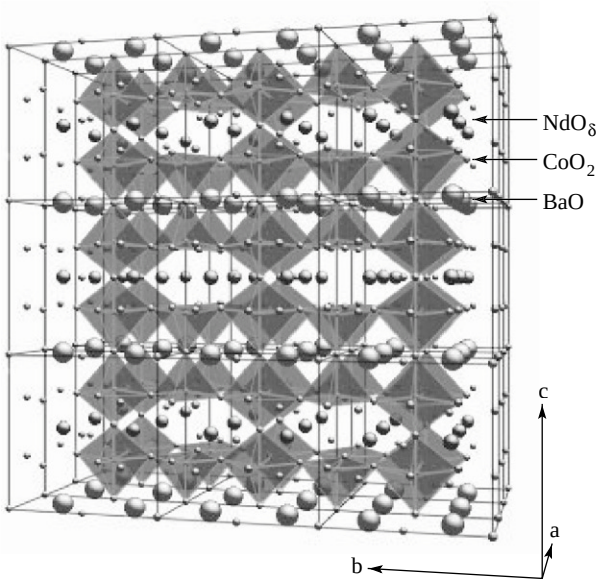

Fig. 1. Crystal structure of LnBaCo$_2$O$_{5+\delta}$, $\delta = 0.5$, with ordered oxide vacancies.

powder diffraction study. Further, the charge ordering (Co^{2+}/Co^{3+}) was inferred from the difference in magnetic moment of ca. 1 μ_B between the two crystallographically distinct Co sites and an associated resistivity anomaly. For $\delta = 0.5$ (Ln = Nd, Tb, Dy, Gd, Ho, Pr, Y), an insulator–metal transition has been observed on warming, with an associated peak in the magnetization [9,11,12]. This has been suggested to be due to a transition to long-range ferromagnetism [9]; however the moment per Co ion of $\backsim 0.18\ \mu_B$ (as derived from bulk magnetization measurements of YBaCo$_2$O$_{5.5}$) does not appear to support this [13]. The nature of, and driving forces behind, this transition are unclear at present. Given the rich variety of chemistry observed to date in the LnBaCo$_2$O$_{5+\delta}$ system, we undertook the present structural study using neutron powder diffraction with an aim of systematically exploring the structure and magnetism in this class of materials. We chose Nd as the lanthanide, as our preliminary experiments indicated that in this system, as opposed to those of smaller rare-earths, the oxygen content could be easily tuned over a wide range. Magnetic studies have been performed on the Nd$_{1-x}$Ba$_x$Co$_2$O$_{5+\delta}$ system by other workers [14,15]; however, to date a full structural and magnetic study has not been performed.

Our studies reveal a wide range of phenomena as a function of δ, including: (i) the oxide vacancy concentration can be easily tuned, but gross inhomogeneities can result from imprecise synthesis conditions (e.g., poor choice of cooling rate in the final firing); (ii) no long-range charge-order is observed at any composition, notably at $\delta = 0$ (where $Co^{2+}/Co^{3+} = 1$), and (iii) the structurally well-ordered $\delta = 0.5$ compound exhibits weak, short-range magnetic order, in distinct contrast with its structurally disordered but magnetically well-ordered neighbors.

2. Experimental

Black polycrystalline samples of NdBaCo$_2$O$_{5+\delta}$ were prepared by a standard ceramic method. Nd$_2$O$_3$ (Alfa, 99.99%), BaCO$_3$ (Alfa, 99.997%) and Co$_3$O$_4$ (Alfa, 99.9985%), all used as-received apart from Nd$_2$O$_3$ which was dried at 900°C prior to use, were weighed out in the appropriate proportions and ball milled for several hours. Decarbonation for 2 days at 1000°C was followed by repeated firing at 1050°C with intermediate regrindings. The reaction was deemed complete when no further changes and no traces of starting materials were observed in successive X-ray powder diffraction patterns. In order to control oxygen content, samples were annealed under differing oxygen partial pressures and temperatures. All oxygen contents were measured after synthesis by thermogravimetric analyses in a 4% H$_2$/Ar atmosphere, and confirmed through neutron powder diffraction. Our results indicate that the oxygen content and homogeneity in this family of materials is highly synthesis-dependent, with careful choice of cooling rate and atmosphere required to synthesize monophasic materials.

This standard ceramic synthesis of NdBaCo$_2$O$_{5+\delta}$ yielded a material having $0 \leqslant \delta \leqslant 0.7$, depending upon both the rate of cooling and atmosphere employed for the final firing. Air quenching of a powder (i.e. removal of the sample from the furnace and allowing to cool under ambient conditions) typically gave samples having oxygen contents $0.64 \leqslant \delta \leqslant 0.72$, one of which was used for the neutron powder diffraction study reported here. The sample with $\delta = 0.5$ was synthesized by slow cooling a powdered sample from 400°C in an argon atmosphere. Attempts to slow cool a thin pellet ($h = 1$ mm, $\Phi = 10$ mm) yielded a multiphasic material, presumably due to an inhomogeneous oxygen distribution throughout the sample. Quenching from 850°C, 5% O$_2$/Ar atmosphere, into liquid nitrogen produced the sample with $\delta = 0.38$. Due to the configuration of the furnace available for quenching of a powder, a maximum of ca. 1 g of material could be produced per quench, thus in order to obtain samples suitable for neutron diffraction the procedure was repeated four times. Quenching from air into liquid nitrogen from synthesis temperature (1050°C) yields a material having $\delta = 0$; in this case the sample could be successfully synthesized as a pressed pellet.

The samples (each ca. 4 g) were loaded into thin-walled, cylindrical vanadium cans, and time-of-flight neutron powder diffraction patterns were collected as a function of temperature using the special environment powder diffractometer (SEPD) at the Intense Pulsed

Neutron Source at Argonne National Laboratory. Cooling was achieved using a closed cycle refrigerator capable of ca. 15 K. The data were analyzed using routines available within the GSAS package [16], including the Rietveld method [17,18]. The background was fitted using an empirical Chebyshev polynomial. Peak shapes were modeled using a convolution of two back-to-back exponentials with a pseudo-Voigt function. Goodness-of-fit parameters quoted in the text refer to the entire dataset.

Electron diffraction experiments were performed as a function of temperature on the $\delta = 0$ material, using a Philips CM30 electron microscope operated at 300 keV. A small disc was cut from a pressed and sintered pellet, and polished to a thickness of ca. 100 μm. The disc was then dimpled, followed by low-angle ion beam milling to create a small hole surrounded by a thin area in which transmission electron microscopy experiments could be performed. This allowed for good thermal contact with the sample holder. A double-tilt, liquid-nitrogen cooled sample holder was used, with temperature monitored by a thermocouple close to the sample. Temperatures were allowed to stabilize for several minutes prior to collecting electron diffraction patterns.

3. Results

The diffraction profiles of the materials on cooling are shown in Figs. 2 and 3, with a typical Rietveld refinement in Fig. 4. Refined structural parameters are given in Tables 1 and 2. We now discuss the results from the materials with $\delta = 0$, 0.38, 0.5, 0.69.

3.1. $\delta = 0$ (50:50 Co^{2+}:Co^{3+})

The sample can be described as orthorhombic, having lattice parameters $a_p \times a_p \times 2a_p$, and is isostructural with the quasi-two-dimensional $LaBaMn_2O_5$ [19] rather than with the three-dimensional $Sr_2Mn_2O_5$ [20]. We find long-range G-type antiferromagnetic ordering in the temperature range studied, with an estimated Néel temperature of ca. 400 K. From the refined magnetic moment (3.50(1) μ_B/Co at 15 K), we conclude that the magnetic struture is well-ordered and that both Co^{2+} and Co^{3+} are in the high-spin state, even at 15 K. We observe a smooth variation of the moment with temperature, suggesting the absence of 'spin crossover' behavior as reported for $YBaCo_2O_5$ [21]. We find no compelling evidence of long-range charge ordering; however as discussed below we do observe a slight anomaly in the resistivity around the temperature at which long-range charge ordering was observed in $LnBaCo_2O_5$ (Ln = Tb, Dy, Gd) [22].

At room temperature, the diffraction pattern can be indexed on the basis of an $a_p \times a_p \times 2a_p$ pseudo-

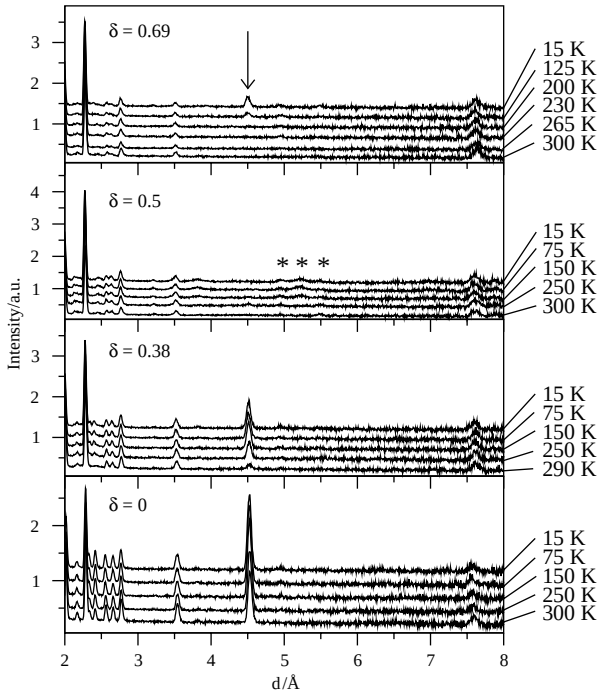

Fig. 2. Observed neutron powder diffraction profiles for $NdBaCo_2O_{5+\delta}$ for the conditions and values of δ given. For clarity, the data are presented as lines joining data points. The arrow indicates a G-type magnetic reflection; the stars indicate the diffuse magnetic scattering for $NdBaCo_2O_{5.5}$.

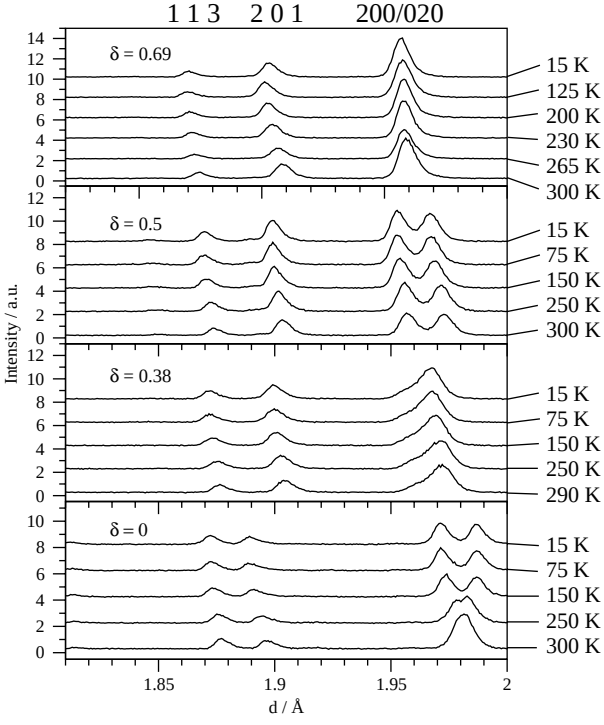

Fig. 3. Observed neutron powder diffraction profiles for backscattering detector bank (highest resolution) for $1.82 \leqslant d \leqslant 2$ Å. The indexing refers to the '$(a_p \times a_p \times 2a_p)$' cell.

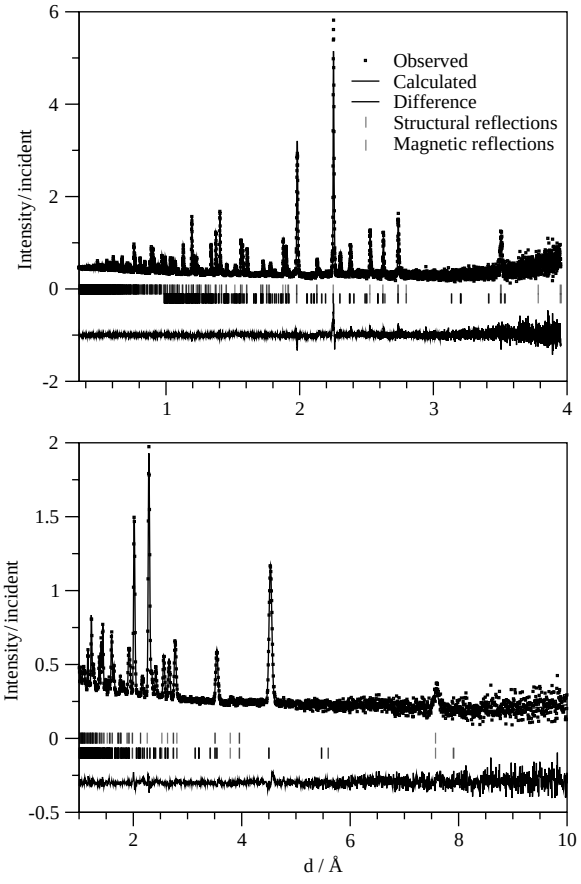

Fig. 4. Results of Rietveld analysis of $NdBaCo_2O_5$ at room temperature, using the backscattering (upper) and 44° (lower) detector banks. $\chi^2 = 1.481$, $R_{wp} = 5.18\%$, $R_p = 3.24\%$, DW-$d = 1.461$, 57 variables. Three banks of data were used for each structural refinement.

tetragonal structural unit cell, and a magnetic cell of $2a_p \times 2a_p \times 2a_p$. However on cooling to 15 K, a distinct orthorhombic distortion is evidenced, in particular by the splitting of the 200/020 doublet at $d/\text{Å} \approx 1.98$ (Fig. 3). Rietveld refinements were performed using a model in which the doubling of the c parameter with respect to the basic perovskite cell was accounted for by ordering of Ba^{2+} and Nd^{3+} into layers perpendicular to z. The magnetic scattering was described using a G-type antiferromagnetic model, in which all nearest-neighbor Co–Co interactions are antiferromagnetic. The refinements converged swiftly to give acceptable fits with chemically reasonable refined parameters. All of the oxide vacancies were found to lie within the NdO_δ planes. A difference Fourier analysis gave no indication of any oxygen on the (0, 0, 0) position. We note, however, that the atomic displacement parameters (ADPs) of the axial O2 oxide ion, although decreasing smoothly on cooling, are not compatible with standard vibrational motion in perovskites (in which the bond bending component is greater than the bond stretching) but rather are suggestive of static displacements incoherent with the cell and space group used in this study. However the use of alternative space groups and cells (e.g. Pmmb, $a_p \times 2a_p \times 2a_p$) did not lead to a significant reduction in the magnitude of the displacement.

The refined moment at room temperature was 2.56(1) μ_B per Co ion, increasing smoothly on cooling to 3.50(1) μ_B at 15 K (Fig. 5). This observation suggests (assuming $g \approx 2$) that both Co^{2+} and Co^{3+} are in a high-spin state (Co^{2+}, $S = \frac{3}{2}$, Co^{3+}, $S = 2$). Here we assume that the orbital contribution to the total moment of both ions is roughly canceled by the effects of covalency, zero-point motion, etc. This refined moment and concomitant assigment of spin state is in accordance with studies performed on $LnBaCo_2O_5$ (Ln = Ho, Tb, Dy) [22], but is in contrast to studies on $YBaCoCu_{0.5}Fe_{0.5}O_5$, in which it was suggested, on the basis of neutron powder diffraction and Mössbauer spectroscopy, that the Co^{3+} was in the intermediate-spin state [23]. Also, in $YBaCo_{2-x}Cu_xO_5$ the Co^{3+} is said to adopt the IS state [24]. These observations suggest that further studies of the $LnBa_2CoO_5$ family are likely to uncover novel spin-state phenomena.

The variation of the refined moment with temperature suggests that the Néel temperature T_N is around 380 K, although our lack of data above room temperature places some limits on the accuracy of this estimate. For spin crossover as reported for $YBaCo_2O_5$ [21], we would expect to see an anomaly in the variation of moment with temperature. The observed behavior is smooth within the temperature range studied, providing no evidence for a spin crossover in the present case. The moments lie parallel to the y-axis, with trial refinements in which the moments are directed in x- and z-axis giving far poorer fits to the data.

No Bragg peaks indicative of charge order were observed at any temperature in our datasets. Refinements in which charge ordering of the type observed by Fauth et al. [22], or expanded unit cells (e.g., $a_p \times 2a_p \times 2a_p$) were allowed did not result in a significant improvement in the description of the observed scattering. Attempts to refine the magnetic structure in a two-sublattice ferrimagnetic (charge-ordered) model converged with both sub-lattices having the same moment within experimental uncertainty. The ADPs of the oxide ions were reduced smoothly on cooling, indicating that no space group-incoherent displacements occurred in the temperature range studied (which might be expected be be present for a charge ordered structure refined in the space group used in this study), within the accuracy of our data.

The electrical resistivity was investigated in light of the reports of charge ordering at $T_{CO} \approx 210$ K in $LnBa_2CoO_5$ (Ln = Tb, Dy, Ho) [22], and is reported in Fig. 6. The sample having $\delta = 0$ was the only one which could be successfully sintered to yield a material with

Table 1
Refined structural parameters for $NdBaCo_2O_{5+\delta}$ with $\delta = 0$, 0.37

T(K)		15	75	150	250	300	15	75	150	250	290
δ				0					0.38		
a(Å)		3.96134(5)	3.96159(5)	3.96104(5)	3.95527(6)	3.95376(7)	3.8993(2)	3.8994(2)	3.9020(2)	3.9054(2)	3.9073(2)
							3.9135(2)	3.9140(2)	3.9161(2)	3.9198(2)	3.9221(2)
b(Å)		3.93042(5)	3.93108(5)	3.93441(5)	3.94270(6)	3.94440(7)	3.9253(3)	3.92637(3)	3.9289(3)	3.9344(2)	3.9359(3)
							3.9226(2)	3.9233(3)	3.9258(3)	3.9298(2)	3.9318(2)
c(Å)		7.5332(1)	7.5341(1)	7.5400(1)	7.5528(1)	7.5623(1)	7.5741(6)	7.5708(6)	7.5783(6)	7.5840(7)	7.5908(7)
							7.5693(4)	7.5694(4)	7.5732(4)	7.5830(5)	7.5894(4)
Volume (Å^3)		117.290(2)	117.331(2)	117.506(2)	117.782(2)	117.935(2)	115.93(1)	115.98(1)	116.18(1)	116.53(1)	116.734
							116.199(7)	116.234(7)	116.430(7)	116.807(8)	117.033(8)
Nd											
	U_{iso}(Å)	0.26(1)	0.29(2)	0.39(2)	0.55(2)	0.62(2)	1.03(5)	1.09(5)	1.18(5)	1.21(5)	1.22(6)
Ba											
	U_{iso}(Å)	0.37(3)	0.43(4)	0.62(4)	0.90(4)	0.94(4)	0.26(5)	0.33(5)	0.42(5)	0.66(6)	0.64(6)
Co											
	z	0.2459(3)	0.2456(3)	0.2455(3)	0.2463(3)	0.2460(3)	0.2480(3)	0.2476(3)	0.2476(4)	0.2473(4)	0.2473(4)
	U_{iso}(Å)	—	—	—	—	0.75(4)	0.46(5)	0.46(4)	0.57(5)	0.66(5)	0.67(5)
	$M(\mu_B)$	3.50(1)	3.50(1)	3.44(1)	3.03(1)	2.56(1)	2.64(3)	2.60(3)	2.60(3)	2.06(3)	1.23(3)
O1											
	z	0.1974(3)	0.1982(3)	0.1978(4)	0.1956(5)	0.1952(5)	0.2119(6)	0.2034(4)	0.2127(5)	0.2120(6)	0.2128(6)
	U_{11}	0.68(7)	0.59(7)	0.70(7)	0.66(9)	0.39(9)	0.9(2)	1.0(1)	1.0(1)	1.0(1)	1.0(2)
	U_{22}	0.64(7)	0.56(7)	0.56(7)	1.1(1)	1.3(1)	1.1(1)	1.1(1)	1.3(1)	1.2(1)	1.4(2)
	U_{33}	0.5(1)	0.9(1)	1.2(1)	0.6(1)	0.8(1)	2.6(2)	2.9(2)	3.0(2)	3.0(2)	3.1(2)
O2											
	z	0.1980(3)	0.1971(3)	0.1972(3)	0.1998(5)	0.1998(6)	0.2039(5)	0.2034(4)	2.038(5)	0.2038(5)	0.2033(5)
	U_{11}	1.18(8)	1.26(8)	1.34(8)	1.1(1)	1.0(1)	1.9(2)	2.0(2)	2.2(2)	2.3(2)	2.2(2)
	U_{22}	0.39(6)	0.50(6)	0.55(7)	0.8(1)	1.2(1)	0.6(1)	0.7(1)	0.7(1)	1.0(1)	1.1(1)
	U_{33}	0.8(1)	0.5(1)	0.5(1)	1.5(2)	1.5(2)	0.7(1)	0.6(1)	0.8(1)	1.0(1)	1.0(1)
O3											
	U_{11}	0.57(8)	0.63(9)	1.0(1)	1.1(1)	1.4(2)	1.3(2)	1.6(2)	1.7(2)	1.6(2)	1.8(2)
	U_{22}	1.00(9)	1.03(9)	0.96(9)	1.6(2)	1.3(2)	0.9(2)	0.9(2)	1.0(2)	1.0(2)	1.3(1)
	U_{33}	0.46(6)	0.50(6)	0.51(7)	0.52(7)	0.48(7)	0.34(8)	0.29(8)	0.36(8)	0.32(8)	0.37(9)
O4											
	Occupancy	0	0	0	0	0	0.52(4)	0.53(4)	0.50(4)	0.48(4)	0.51(4)
							0.31(2)	0.29(2)	0.31(2)	0.32(2)	0.30(2)
	U_{iso}						1.0(2)	1.0(2)	1.0(2)	1.0(2)	0.9(2)
Co–O1(Å)		1.9990(6)	1.9978(6)	1.9998(6)	2.0082(9)	2.001(1)	1.9802(6)	1.9809(6)	1.9821(6)	1.9853(7)	1.9852(6)
							1.9816(7)	1.9793(6)	1.9806(6)	1.9830(7)	1.9832(6)
Co–O2(Å)		2.0133(6)	2.0143(6)	2.0138(7)	2.0086(7)	2.0069(8)	1.9849(8)	1.9872(8)	1.9781(8)	1.9804(8)	1.9819(9)
							1.9779(8)	1.9854(8)	1.9860(8)	1.9875(8)	1.9892(9)
Co–O3(Å)		1.914(2)	1.916(2)	1.919(2)	1.916(3)	1.860(2)	1.908(3)	1.912(3)	1.913(3)	1.916(3)	1.918(3)
							1.909(1)	1.911(3)	1.912(3)	1.916(3)	1.918(3)
Co–O4(Å)		—	—	—	—	—	1.876(3)	1.876(3)	1.875(3)	1.876(3)	1.877(3)
							1.877(3)	1.874(3)	1.875(3)	1.876(3)	1.877(3)
O1–Co–O1 (deg)		158.9(2)	159.4(2)	159.3(2)	158.0(3)	157.9(3)	164.2(3)	164.7(3)	164.7(3)	164.5(3)	164.8(3)
							164.2(3)	164.7(3)	164.7(3)	164.5(3)	164.8(3)
O2–Co–O2 (deg)		159.4(2)	159.1(2)	159.1(2)	160.1(3)	159.9(2)	160.6(3)	160.5(3)	160.7(3)	160.8(3)	160.6(3)
							160.6(3)	160.6(3)	160.8(3)	160.9(3)	160.7(3)
χ^2		1.615	1.597	1.519	1.464	1.502	1.967	1.938	1.914	1.802	1.704
R_{wp}		5.31	5.26	5.11	5.02	4.77	5.45	5.51	5.37	5.20	5.22
R_p		3.44	3.42	3.32	3.21	3.07	3.79	3.73	3.67	3.53	3.55
DW–d		1.365	1.359	1.400	1.410	1.502	1.119	1.123	1.125	1.178	1.279

All ADPs (U) are given as 100 times the actual value. Space group *Pmmm*: Nd 1*f*; Ba 1*h*; Co 2*q*; O1 2*r*; O2 2*s*; O3 1*c*; O4 1*a*.

acceptable oxygen homogeneity, indicating the difficulties inherent in preparing single-phase samples of this structural family. The resistivity may be phenomenologically described over the entire temperature range studied using a variable-range hopping (VRH) model $\rho_{vrh} = \rho_0 \exp((T_0/T)^{1/4})$. The fit yields a density of states at the Fermi level $N(E_F)$ of ca. 2×10^{18} cm^{-3}, which is in full agreement with the value obtained by Fauth et al. for similar systems [22]. Fits to models for activated behavior, and small polaron behavior, did not describe the data well. However, a close inspection of the data suggests the presence of three regions: one at

Table 2
Refined structural parameters for $NdBaCo_2O_{5+\delta}$ with $\delta = 0.5, 0.69$

T(K)		15	75	150	250	300	15	125	200	230	265	300
δ				0.5						0.69		
a(Å)		3.89241(4)	3.89253(4)	3.89447(4)	3.89835(4)	3.90049(4)	3.89700(9)	3.89788(7)	3.89935(8)	3.89997(9)	3.9002(1)	3.90124(7)
b(Å)		7.84045(9)	7.84157(9)	7.84689(9)	7.85805(9)	7.86355(9)	7.8041(2)	7.8087(2)	7.8090(2)	7.8093(2)	7.8106(2)	7.8156(2)
c(Å)		7.56989(9)	7.57009(9)	7.57276(9)	7.57987(9)	7.5867(1)	7.58482(9)	7.57867(9)	7.58326(9)	7.59006(9)	7.5987(1)	7.60671(9)
Volume (Å^3)		231.020(3)	231.066(3)	231.420(3)	232.197(3)	232.700(4)	230.674(3)	230.674(3)	230.913(3)	231.162(3)	231.476(4)	231.931(3)
Nd												
	y	0.2710(2)	0.2710(2)	0.2707(2)	0.2709(2)	0.2700(3)	0.2633(4)	0.2638(4)	0.2638(4)	0.2634(4)	0.2645(5)	0.2624(4)
	U_{iso}/Å	0.31(3)	0.35(3)	0.35(3)	0.44(3)	0.54(4)	0.39(4)	0.48(3)	0.52(3)	0.67(3)	0.65(4)	0.80(4)
Ba												
	y	0.2498(3)	0.2499(3)	0.2499(3)	0.2500(3)	0.2506(4)	0.2515(5)	0.2519(4)	0.2511(5)	0.2515(5)	0.2515(6)	0.2516(5)
	U_{iso}(Å)	0.09(3)	0.14(4)	0.20(4)	0.41(4)	0.47(5)	0.19(4)	0.09(3)	0.14(3)	0.18(3)	0.26(4)	0.28(3)
Co1												
	z	0.2466(6)	0.2466(6)	0.2472(6)	0.2475(6)	0.2468(7)	0.2485(8)	0.2476(8)	0.2481(9)	0.2480(9)	0.249(1)	0.249(9)
	U_{iso}(Å)	0.09(3)	0.41(7)	0.35(7)	0.63(8)	0.47(8)	0.37(9)	0.32(9)	0.4(1)	0.5(1)	0.4(1)	0.6(1)
Co2												
	z	0.2554(6)	0.2548(6)	0.2551(6)	0.2548(6)	0.2550(7)	0.2531(9)	0.2541(9)	0.2541(9)	0.2537(9)	0.255(1)	0.2535(9)
	U_{iso}(Å)	0.26(6)	0.32(6)	0.37(7)	0.39(7)	0.64(9)	0.34(9)	0.44(9)	0.5(1)	0.5(1)	0.6(1)	0.6(1)
	$M(\mu_B)$	—	—	—	—	—	1.39(2)	0.89(2)	—	—	—	—
O1												
	U_{iso}(Å)						0.66(8)	0.97(2)	1.04(2)	1.12(2)	1.19(2)	1.25(2)
O2												
	U_{iso}(Å)						0.73(9)	0.97(2)	1.04(2)	1.12(2)	1.19(2)	1.25(2)
O1, O2												
	U_{11}	0.99(9)	0.88(9)	1.2(1)	1.1(1)	1.3(1)						
	U_{22}	0.7(1)	0.7(1)	0.7(1)	0.9(1)	0.7(1)						
	U_{33}	0.48(6)	0.44(6)	0.47(6)	0.45(7)	0.57(8)						
O3												
	U_{iso}(Å)						0.9(1)	0.97(2)	1.04(2)	1.12(2)	1.19(2)	1.25(2)
	U_{11}	0.8(1)	0.8(2)	0.8(2)	1.2(2)	1.1(2)						
	U_{22}	0.7(1)	0.9(1)	1.2(2)	1.2(2)	1.5(2)						
	U_{33}	0.0(1)	0.1(1)	0.0(1)	0.3(1)	0.3(1)						
O4												
	z	0.3052(4)	0.3067(4)	0.3069(4)	0.3073(4)	0.3061(5)	0.2969(7)	0.2981(6)	0.2962(7)	0.2945(7)	0.2942(8)	0.2390(6)
	U_{iso}(Å)						1.31(9)	0.97(2)	1.04(2)	1.12(2)	1.19(2)	1.25(2)

	U_{11}	1.7(1)	1.8(1)	1.8(1)	1.9(2)	1.7(2)						
	U_{22}	0.6(1)	0.6(1)	0.6(1)	0.8(1)	0.8(1)						
	U_{33}	0.9(1)	0.7(1)	0.9(1)	0.9(1)	1.5(2)						
O5												
	z	0.2674(3)	0.2671(4)	0.2681(4)	0.2688(4)	0.2675(5)	0.2637(5)	0.2644(6)	0.2648(6)	0.2630(5)	0.2634(6)	0.2619(5)
	U_{iso}(Å)						0.74(6)	0.97(2)	1.04(2)	1.12(2)	1.19(2)	1.25(2)
	U_{11}	0.75(9)	0.73(9)	0.55(9)	0.7(1)	0.8(1)						
	U_{22}	0.4(1)	0.4(1)	0.6(1)	0.7(1)	1.2(2)						
	U_{33}	0.7(1)	0.9(1)	0.9(1)	1.1(1)	1.1(1)						
O6												
	y	0.2412(3)	0.2412(2)	0.2408(3)	0.2412(3)	0.2407(3)	0.2432(4)	0.2435(4)	0.2431(4)	0.2433(4)	0.2428(5)	0.2427(4)
	z	0.2881(3)	0.2876(3)	0.2870(3)	0.2862(3)	0.2872(4)	0.2857(5)	0.2835(5)	0.2839(5)	0.2854(5)	0.2855(5)	0.2868(4)
	U_{iso}(Å)						1.00(6)	0.97(2)	1.04(2)	1.12(2)	1.19(2)	1.25(2)
	U_{11}	0.38(6)	0.42(6)	0.54(6)	0.68(7)	0.83(8)						
	U_{22}	1.38(8)	1.41(8)	1.49(8)	1.64(9)	1.7(1)						
	U_{33}	0.94(7)	0.87(7)	1.08(8)	1.32(9)	1.2(1)						
	U_{23}	−0.55(6)	−0.57(6)	−0.61(7)	−0.73(8)	−0.67(9)						
O7												
	U_{iso}(Å)	—	—	—	—	—	1.9(4)	0.97(2)	1.04(2)	1.12(2)	1.19(2)	1.25(2)
	Occupancy	—	—	—	—	—	0.39(1)	0.379(9)	0.385(9)	0.397(9)	0.39(1)	0.395(9)
Co1–O2(Å)		1.867(4)	1.867(4)	1.872(4)	1.876(5)	1.873(5)	1.885(6)	1.876(6)	1.881(7)	1.883(7)	1.888(7)	1.892(7)
Co1–O3(Å)		1.918(4)	1.918(4)	1.915(4)	1.914(5)	1.921(5)	1.908(6)	1.913(6)	1.910(7)	1.913(7)	1.911(7)	1.911(7)
Co1–O5(Å)		1.9525(4)	1.9524(4)	1.9537(4)	1.9559(5)	1.9565(5)	1.9519(4)	1.9531(5)	1.9538(5)	1.9533(4)	1.9534(5)	1.9532(4)
Co1–O6(Å)		2.053(2)	2.053(2)	2.056(2)	2.055(2)	2.061(2)	2.024(3)	2.021(3)	2.025(3)	2.024(3)	2.029(4)	2.032(3)
Co2–O1(Å)		1.933(4)	1.929(4)	1.932(4)	1.931(5)	1.935(5)	1.919(7)	1.925(7)	1.927(7)	1.926(7)	1.939(8)	1.929(7)
Co2–O4(Å)		1.983(1)	1.986(1)	1.986(1)	1.989(1)	1.988(1)	1.9767(2)	1.977(2)	1.976(2)	1.975(2)	1.973(2)	1.984(1)
Co2–O6(Å)		1.908(2)	1.908(2)	1.905(2)	1.910(2)	1.909(3)	1.914(3)	1.914(3)	1.912(3)	1.915(3)	1.910(4)	1.914(3)
Co2–O7(Å)		—	—	—	—	—	1.873(7)	1.864(7)	1.865(7)	1.869(7)	1.860(8)	1.875(7)
O5-Co1-O5(deg)		170.7(3)	170.9(3)	170.7(3)	170.5(3)	170.8(4)	173.2(4)	172.5(4)	172.6(4)	173.3(4)	173.4(5)	174.2(4)
O6-Co1-O6(deg)		162.4(3)	159.1(2)	163.1(3)	163.6(3)	162.9(3)	164.0(4)	164.5(4)	164.6	163.9(5)	164.1(5)	163.6(4)
O4-Co2-O4(deg)		158.0(2)	157.2(3)	157.3(3)	156.9(3)	157.5(4)	160.6(5)	160.6(5)	161.4(5)	161.9(5)	162.7(6)	162.5(5)
O6-Co2-O6(deg)		165.1(3)	165.1(3)	165.4(3)	165.7(3)	165.3(4)	165.2(4)	166.6(4)	166.4(4)	165.6(4)	166.1(5)	164.8(4)
χ^2		1.823	1.794	1.715	1.626	1.481	1.578	1.496	1.465	1.437	1.386	1.465
R_{wp}(%)		5.12	5.07	4.97	4.85	5.18	5.50	5.350	5.280	5.26	5.72	5.08
R_p(%)		3.28	3.22	3.19	3.12	3.24	3.58	3.52	3.49	3.45	3.67	3.32
DW-d		1.190	1.210	1.285	1.332	1.461	1.386	1.430	1.456	1.471	1.543	1.454

All ADPs (U) are given as 100 times the actual value. Space group *Pmmm*: Nd 2*p*; Ba 2*o*; Co1 2*r*; Co2 2*q*; O1 1*a*; O2 1*e*; O3 1*g*; O4 2*s*; O5 2*t*; O6 4*u*; O7 1*c*.

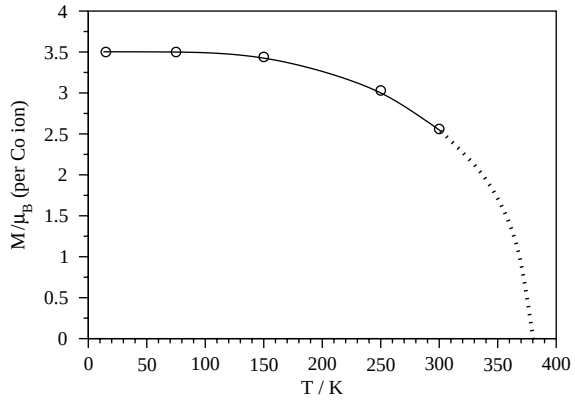

Fig. 5. Variation in refined magnetic moment per Co ion for $NdBaCo_2O_5$ on cooling. The line is to guide the eye; standard deviations are smaller than the data points.

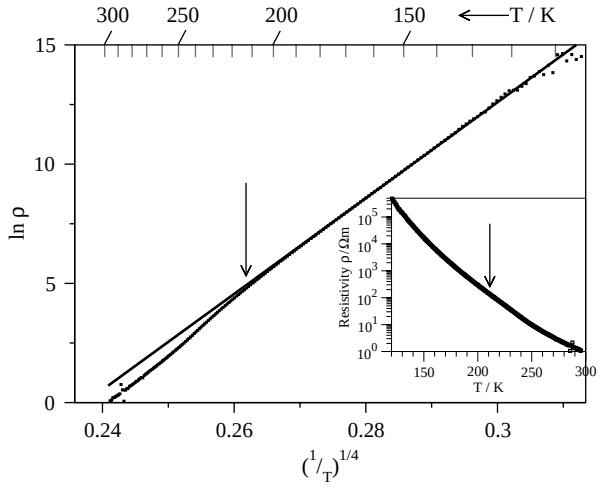

Fig. 6. Variable-range hopping (VRH) plot for $NdBaCo_2O_5$; the straight line is a fit to the VRH model. The resistivity is shown in the inset. Arrows are drawn to indicate the deviation in the resistivity at ca. 210 K.

higher temperatures, one at lower, and a crossover. In Fig. 6, a fit to the VRH model is shown for $0.27 \leqslant T^{\frac{1}{4}} \leqslant 0.31\ \mathrm{K}^{\frac{1}{4}}$, and as such emphasizes this small anomaly. The deviation from VRH behavior at $T \approx 210$ K is reminiscent of that for $HoBaCo_2O_5$ as reported by Fauth et al., which was shown to be due to charge-ordering between Co^{2+} and Co^{3+} [22].

To further investigate the possibility of charge ordering in the $\delta = 0$ compound, electron diffraction measurements were performed as a function of temperature. On cooling, no marked changes in the [0 0 1] zone axis pattern indicative of charge ordering occurred, such as the appearance of extra reflections or diffuse scattering (Fig. 7). From this observation we conclude that the weak feature in the resistivity is not due to long-range charge ordering, or perhaps that charge ordering occurs in only a small fraction of the sample, below the

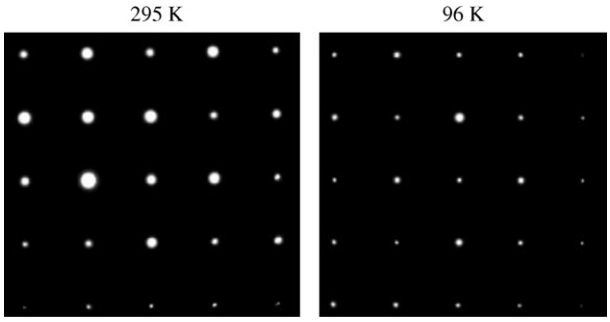

Fig. 7. [001] zone axis diffraction patterns of $NdBaCo_2O_5$ at 295 and 96 K.

detection limits of our electron microscopy study. We thus find no compelling evidence of charge ordering in $NdBaCo_2O_5$.

3.2. $\delta = 0.38$ (12:88 Co^{2+}:Co^{3+})

The structure is derived from that of the $\delta = 0$ material, with oxygen ions inserted at random (within the resolution of our data and technique) into the NdO_δ layer. We again find long-range G-type antiferromagnetic ordering in the temperature range studied, with an estimated Néel temperature of ca. 150 K. As a result of the synthetic procedure the sample is multiphasic, which limits the information we are able to obtain about this composition. However, the magnetic structure and moment are well accounted for assuming that the spin state of the Co^{3+} is determined by the magnitude of the local crystal field as determined by the co-ordination geometry.

At room temperature, the pattern could be indexed in a similar manner to that of the $\delta = 0$ sample. However, inspection of the Bragg reflection profiles, especially that at ca. 1.98 Å which exhibited a 'shoulder' at lower d-spacing (Fig. 3), suggested that this sample could not be described as monophasic. This is likely to be a result of the multiple batch synthetic procedure. Accordingly, three approaches were taken to account fully for these data. Our models comprised of two structural phases, with a magnetic moment being associated with either or both. The model in which both phases were magnetic proved unstable; this is likely to be due either to the limited resolution of our data at higher d-spacings, or to the lack of magnetic scattering in one of the phases. The overall oxygen content refined to an average of 5.38(5), in good agreement with the TGA result of 5.37(1). The two phases were constrained to be identical structurally, apart from the oxygen content, which refined to a value of 5.29(2) for the majority phase, and 5.50(4) for the minority phase. Although the two trial refinements in which the moment was tied to one phase, then the other, were able to describe the observed data equally well, we assume that the moment is associated with the phase

having $\delta = 0.29(2)$, in accordance with our model of $NdBaCo_2O_{5.5}$ (vide infra). Further studies, including the synthesis of a homogeneous material with $\delta = 0.3$, are underway.[1]

On cooling, the intensity of the magnetic Bragg reflections increased dramatically, with the moment refining to $1.23(3)\,\mu_B$ per Co ion at 295 K, and $2.64(3)\,\mu_B$ at 15 K. Note that the assignment of magnetic scattering to only one of the two phases places some limits on the reliability of this refined moment. Simple assumptions for the spin states, namely that the octahedral Co^{3+} is low spin as in Co_3O_4 and that the square-pyramidal Co^{3+} and Co^{2+} are high spin as in the $\delta = 0$ material, predict a moment of $2.63\,\mu_B$ per Co ion for the magnetic $\delta = 0.29$ phase.[2] This value corresponds well with that observed ($2.64(3)\,\mu_B$ per Co). From a consideration of the Goodenough-Kanomori rules [25,26], the magnetic structure in the assumed spin states is expected to be *G*-type antiferromagnetic, as is observed.

3.3. $\delta = 0.5$ (Co^{3+})

Observation of $(0, \frac{1}{2}, 0)$ superstructure reflections indicates that the cell is orthorhombic, having lattice parameters $a_p \times 2a_p \times 2a_p$. This is due to ordering of oxide vacancies into channels perpendicular to *y*, which is in contrast to the ordering pattern in the corresponding manganite $LaBaMn_2O_{5.5}$ [27]. The sample studied presents no evidence of long-range magnetic order. Weak, diffuse scattering at high *d*-spacings is observed on cooling, with a change in the position between 200 and 250 K.

The diffraction pattern collected at room temperature could not be indexed on the basis of the $a_p \times a_p \times 2a_p$ structural unit cell used for $\delta < 0.5$; rather an expanded cell of size $a_p \times 2a_p \times 2a_p$ was required. A structural model of space group *Pmmm* in which the cell doubling in *b* arises from ordering of oxide ion vacancies into channels was successful in fitting the observed patterns. This ordering motif is different from that observed in similar manganites [19,27], and also from that observed in $Sr_2Mn_2O_5$ [20]. The occupancy of the O7 site refined to zero and was fixed at that value; this is in agreement with the TGA result of $\delta = 0.52(1)$.

The Co–O co-ordination environment is markedly distorted compared to the materals with $\delta < 0.5$, with differences between long and short Co–O *xy*-plane bonds being approximately 0.05 Å. This pattern of bond lengths alternation is in agreement with studies by Moritomo of $TbBa_2CoO_{5.5}$ [9]. In this material, both the square-pyramidal and octahedrally co-ordinated Co^{3+} ions were suggested to be in the intermediate spin (IS) state; later these researchers suggested that only the square pyramidally co-ordinated Co^{3+} ions adopt the IS state, with the octahedral Co^{3+} ions in the low-spin state [10]. In the former case, a *C*-type magnetic structure would be expected based on the Goodenough–Kanomori rules; this is not observed. The latter suggestion is in accordance both with the lack of magnetic Bragg scattering observed in this study and with that of $TbBaCoO_{5.5}$; however, comparison with $NdBaCo_2O_5$ suggests that the low-T spin configuration at the square pyramidal sites is high-spin. Further work will be necessary to distinguish between these hypotheses.

No magnetic Bragg scattering was apparent either at room temperature, or on cooling; however, weak, diffuse scattering was observed as shown in Fig. 2. A change in the positions of this scattering was noted on cooling below ca. 200 K. The smallest cell expansions which could account for these diffuse reflections are $2\sqrt{2}a_p \times 2\sqrt{2}a_p \times 2a_p$ for $300 \geqslant T \geqslant 250$ K and $2\sqrt{2}a_p \times 2\sqrt{2}a_p \times 4a_p$ for $T \leqslant 200K$. The weakness and breadth of these features precludes any attempt at a meaningful analysis. Further work is in progress to elucidate the nature of the magnetic behavior in $NdBaCo_2O_{5.5}$, in particular the study of samples with differing degrees of oxide vacancy ordering.

We note that the appearance of magnetic scattering implies that the IS or HS states must be significantly populated in $NdBaCo_2O_{5.5}$ over the temperature range studied. This is to be contrasted to $LaCoO_3$, in which Co also adopts the 3+ oxidation state, but appears to be low spin for $T \leqslant 60\,K$ (e.g. Ref. [4]). This difference in spin states between the isoelectronic $LaCoO_3$ and $NdBaCo_2O_{5.5}$ is likely to be a result of the reduced crystal field for the square-pyramidal, five co-ordinate Co^{3+} in $NdBaCo_2O_3$ (50% of the Co^{3+} ions) compared to the octahedrally co-ordinated Co^{3+} in $LaCoO_3$. This unexpected lack of magnetic order can be explained as being a direct consequence of the layered crystal structure, in which intact, non-magnetic octahedral *ac* layers interleave with magnetic square pyramidal layers. This lamellar structure presumably interrupts the establishment of long range order. The exchange coupling between these HS (or IS) Co^{3+} centers across the 'gap' formed by the ordered oxide vacancies will determine whether the Co–Co interactions are 1*D* (weak coupling) or 2*D* (strong coupling). In the limit of weak coupling, it

[1] We note that our model for $NdBaCo_2O_{5.5}$ is tetragonal in this two-phase study, but orthorhombic for a study of single-phase material. Two-phase refinements in which the $\delta = 0.5$ material was included as orthorhombic were not stable, presumably as a result of the strong overlap of peak positions of the two phases. However, the tetragonal model may not be unreasonable, given the different synthetic procedures for the present sample and the monophasic material, and studies by Akahoshi of $YBaCo_2O_{5.5}$ in which oxide vacancy ordered (orthorhombic) and disordered (tetragonal) materials with $\delta = 0.5$ were prepared, this may not be an unreasonable result [12].

[2] 21% $Co^{2+} = 0.21 \times 3\,\mu_B$; 29% octahedral $Co^{3+} = 0.29 \times 0\,\mu_B$; 50% square-pyramidal $Co^{3+} = 0.5 \times 4\,\mu_B$: total moment $= 2.63\,\mu_B$ per Co ion.

is possible that a spin ladder results. Experiments are in progress to further investigate this hypothesis, in particular the use of inelastic neutron scattering to determine whether a spin gap opens on cooling.

3.4. $\delta = 0.69$ (81:19 Co^{3+}:Co^{4+})

Broadening of reflections with an $h\,k$ component, and observation of very weak $(0\frac{1}{2}0)$ superstructure reflections, indicate that the unit cell for $NdBaCo_2O_{5.69}$ is orthorhombic rather than tetragonal. Refinements suggest that this is due to preferential ordering of oxide vacancies into channels. On cooling, *G*-type magnetic scattering is observed for $T \leqslant 125$ K, with a refined moment per Co ion of 1.42(2) μ_B. The magnitude of the moment can be accounted for in the same manner as for the materials with $\delta \leqslant 0.5$; however, with these spin-state assignments, ferromagnetism is expected. The observed antiferromagnetism can be rationalized on the basis of a model favoring $d_{3z^2-r^2}$ orbital polarization. However in this scenario, the magnitude of the moment is not predicted correctly using the simple models described earlier.

The room temperature dataset could be indexed using a primitive tetragonal cell of dimensions $a_p \times a_p \times 2a_p$. However, trial refinements using this cell suggested that the widths of certain peaks, in particular the (200)/(020), could not be accounted for successfully using this model. Closer inspection also revealed the presence of an extremely weak reflection at the $(1\frac{3}{2}1)$ position, indicating a doubling of the basic cell in the *b* direction. Refinements in the expanded cell, using the *Pmmm* space group, resulted in an improved description of the observed scattering, although ADPs had to be constrained by element and could not be refined anisotropically. This is presumably due to the pseudo-tetragonal nature of the structure. No separation of the (200)/(020) manifold was observed on cooling, in contrast to the material with $\delta = 0$. Unlike samples with other values of δ, the *c*-axis expands slightly on cooling below 125 K (see, for example, the displacement of the 201 reflection with respect to the 200 in Fig. 3, and the change in lattice parameters with temperature shown in Fig. 8).

A model in which the oxide vacancies were disordered in the *xy* plane converged to give $\chi^2 = 1.642$, $R_{wp} = 5.38\%$, $R_p = 3.64\%$, DW-$d = 1.327$, and a model in which the vacancies were preferentially ordered into channels along *a* gave $\chi^2 = 1.465$, $R_{wp} = 5.08\%$, $R_p = 3.32\%$, DW-$d = 1.454$ (both 60 variables). Also, X-ray powder diffraction data (not shown here) indicate a doubling of the *b*-axis, which we take to indicate a weak ordering of the oxide vacancies perpendicular to this direction. This doubling is less evident in neutron diffraction due to the lower effective flux at high *d*-spacings but is nonetheless present; for example the $(1\frac{3}{2}1)$ reflection (based on the $a_p \times a_p \times 2a_p$ cell) at ca. 2.08 Å is weak but present in our data. Thus, a model in which the vacancies are ordered into channels perpendicular to the *b* direction is preferred. The oxygen content refined to 5.69(1), in agreement with the TGA result of 5.67(1).

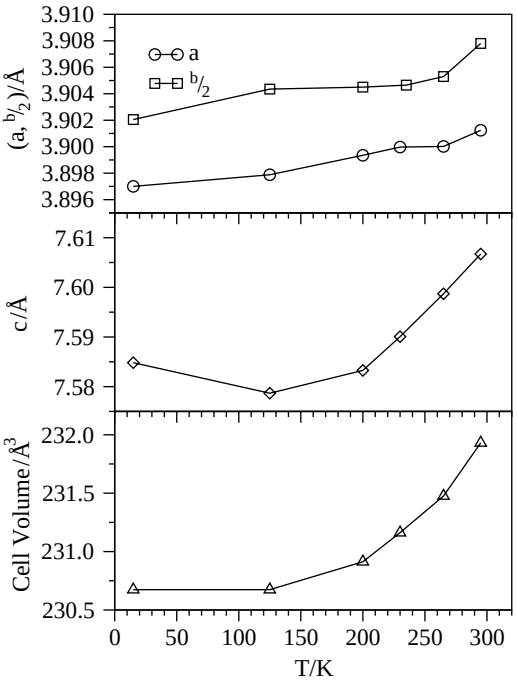

Fig. 8. Variation of lattice parameters and cell volume of $NdBaCo_2O_{5.69}$ as a function of temperature. Error bars are smaller than the points; lines are merely to guide the eye.

On cooling to 125 K, Bragg reflections at the $(111)a_p$ position were observed, characteristic of G-type antiferromagnetic order. However, additional very weak reflections also appeared at this temperature; in particular a reflection at 4.9 Å. This is difficult to account for in terms of any cell expansion, or a magnetic impurity phase (e.g., Co_3O_4, T_N ca. 40 K [28], CoO, T_N ca. 280 K [29]). These features are extremely weak, and given the level of agreement between our model and the observed data, it is likely that the 'true' structure involves a small perturbation of our model. The moment at 15 K refined to 1.42(2) μ_B per Co ion. We present two possible models to explain these data.

(i) The magnitude of this moment can again be rationalized assuming a variation in the spin state of Co with crystal field. If the octahedral sites are occupied by low-spin Co^{3+} and Co^{4+} ions and the remaining Co^{3+} ions preferentially occupy the square pyramidal sites in the high-spin state, the predicted moment is 1.43 μ_B per Co ion; this agrees well with the observed moment of 1.42(2) μ_B. However, a consideration of the likely exchange pathways suggests that this arrangement of spin states should produce a ferromagnetic ground state (the HS Co^{3+}:LS Co^{4+} exchange in particular being strongly ferromagnetic), whereas in fact a *G*-type

antiferromagnetic ground state is observed. Also, this model fails to account for the observed increase in the c lattice parameter on cooling below 125 K (not found for other values of δ).

(ii) An alternative model can account for the antiferromagnetism, but it does not fully account for the ordered magnetic moment. In this model, the spin state of the Co^{3+} ion is always intermediate spin (IS) and the Co^{4+} always low spin, both regardless of local coordination geometry. This stabilization of the IS Co^{3+} by LS Co^{4+} has been observed in $La_{1-x}Sr_xCoO_3$ [30]. This model predicts a moment of 1.83 μ_B per Co ion; in this case we must assume that only a part of the material is magnetically ordered. Further, we assume that the Jahn–Teller active IS Co^{3+} preferentially occupies a $d_{3z^2-r^2}$ orbital with its e_g electron upon cooling. With these assumptions, the Co moment is predicted to be 1.83 μ_B per Co, which can be compared to the observed value of 1.42(2) μ_B per Co. With this orbital polarization, the majority of the exchange interactions are antiferromagnetic within the Goodenough–Kanomori framework, with the few unavoidable ferromagnetic interactions rationalizing the reduced moment observed by neutron diffraction. Finally, the c-axis expansion at low temperatures is arises from the $d_{3z^2-r^2}$ orbital polarization.

As neither model presented here satisfactorily explains all of the data, it is clear that further work is required to resolve the issue of the unexpected antiferromagnetism in the $\delta = 0.69$ material, with more comprehensive mapping of the phase diagram of crucial importance.

4. Conclusions

Variable temperature neutron powder diffraction has been performed on a number of compositions in the series $NdBaCo_2O_{5+\delta}$ ($\delta = 0$, 0.38, 0.5, 0.69). Our studies clearly indicate that synthesis must be optimized for each composition to insure homogeneity of oxygen content. This is most clearly demonstrated in the case of the nominally $\delta = 0.38$ sample, which has been modeled as a two-phase ($\delta = 0.29$, 0.5) mixture. The dramatic changes in magnetism as a function of δ highlight the importance of this homogeneity for measuring intrinsic properties of well-characterized samples in this system. As a result of this broad survey, we find that the spin state adopted by Co^{3+} is a strong function of local crystal field. Importantly, we observe no structural (unusual cell volume changes) or magnetic (reduction in ordered moment, change in magnetic structure) anomalies on cooling any of our samples. Accordingly, we conclude that there is no compelling structural or magnetic evidence from neutron diffraction for temperature-dependent spin crossover phenomena in the $NdBaCo_2O_{5+\delta}$ system in the range $15 \leqslant T \leqslant 300\ K$.

Unlike $TbBa_2CoO_5$, $NdBaCo_2O_5$ shows no evidence of long-range charge ordering, as evidenced both by total refined moment on the Co site and by unsuccessful refinements of a two-sublattice structural model. These results indicate that the charge-ordering phenomena is apparently extremely dependent upon the lanthanide size ($Nd^{3+} = 1.163$ Å, $Tb^{3+} = 1.095$ Å [31]).

Perhaps the most unexpected result of this study has been the apparent lack of long-range magnetic order in the $\delta = 0.5$ (all Co^{3+}) sample, which possesses a highly ordered defect structure. This sharply contrasts with its magnetically ordered neighbors, in which considerable oxygen vacancy disorder is observed. Despite this high degree of structural order in the $\delta = 0.5$ sample, the magnetic interactions are apparently largely frustrated, as evidenced by weak, diffuse magnetic scattering. This is rationalized as a result of crystal-field induced spin state ordering of the Co^{3+} ions. Further work is in progress to investigate this hypothesis and to fully map out the phase diagram of this structural family as a function of δ.

Acknowledgments

The submitted manuscript has been created by the University of Chicago as Operator of Argonne National Laboratory ('Argonne') under Contract No. W–31–109–ENG–38 with the U.S. Department of Energy. The U.S. Government retains for itself, and others acting on its behalf, a paid–up, non-exclusive, irrevocable worldwide license in said article to reproduce, prepare derivative works, distribute copies to the public, and perform publicly and display publicly, by or on behalf of the Government.

References

[1] K. Asai, A. Yondea, O. Yokokura, J.M. Tranquada, G. Shirane, K. Kohn, J. Phys. Soc. Jpn. 67 (1998) 290.
[2] T. Saitoh, T. Mizokawa, A. Fujimori, M. Abbate, Y. Takeda, M. Takano, Phys. Rev. B 55 (1997) 4257.
[3] M.A. Korotin, S. Yu Ezhov, I.V. Solovyev, V.I. Asimov, D.I. Khomskii, G.A. Sawatzky, Phys. Rev. B 54 (1996) 5309.
[4] K. Asai, P. Gehring, H. Chou, G. Shirane, Phys. Rev. B 40 (1989) 10982.
[5] R.R. Heikes, R.C. Miller, R. Mazelsky, Physica 30 (1964) 1600.
[6] S. Stølen, F. Grønvold, H. Brinks, T. Atake, H. Mori, Phys. Rev. B 55 (1997) 14103.
[7] E.O. Wollan, H.R. Child, W.C. Koehler, M.K. Wilkinson, Phys. Rev. 112 (1958) 1132.
[8] W.L. Roth, J. Phys. Chem. Solids 25 (1964) 1.
[9] Y. Moritomo, T. Akimoto, M. Takeo, A. Machida, E. Nishibori, M. Takata, M. Sakata, K. Ohoyama, A. Nakamura, Phys. Rev. B 61 (2000) R13325.

[10] H. Kusuya, A. Machida, Y. Moritomo, K. Kato, E. Nishibori, M. Takata, M. Sakata, A. Nakamura, J. Phys. Soc. Jpn. 70 (2001) 3577.
[11] A. Maignan, C. Martin, D. Pelloquin, N. Nguyen, B. Raveau, J. Solid State Chem. 142 (1999) 247.
[12] D. Akahoshi, Y. Ueda, J. Phys. Soc. Jpn. 68 (1999) 736.
[13] D. Akahoshi, Y. Ueda, J. Solid State Chem. 56 (2001) 355.
[14] D.D. Khalyavin, I.O. Troyanchuk, N.V. Kasper, H. Szymczak, J. Exp. Theoret. Phys. 93 (2001) 805.
[15] I.O. Troyanchuk, N.V. Kasper, D.D. Khalyavin, A.N. Chobot, G.M. Chobot, H. Szmczak, J. Phys.: Condensed Matter 10 (1998) 6381.
[16] A.C. Larsen, R.B.V. Dreele, Technical Report LANSCE, MSH805, Los Alamos National Laboratory, 1985.
[17] H.M. Rietveld, Acta Crystallogr. 22 (1967) 151.
[18] H.M. Rietveld, J. Appl. Crystallogr. 2 (1969) 65.
[19] F. Millange, V. Caignert, B. Domengès, B. Raveau, Chem. Mater. 10 (1998) 1974.
[20] T. Mori, K. Inoue, N. Kamegashira, Y. Yamaguchi, K. Ohayama, J. Alloys Comp. 296 (2000) 92.
[21] T. Vogt, P.M. Woodward, P. Karen, B.A. Hunter, P. Henning, A.R. Moodenbaugh, Phys. Rev. Lett. 84 (2000) 2969.
[22] F. Fauth, E. Suard, V. Caignaert, B. Domengés, I. Mirabeau, L. Keller, Eur. Phys. J. B 21 (2001) 163.
[23] L. Barbey, N. Nguyen, A. Ducouret, V. Caignaert, J.M. Grenèche, B. Raveau, J. Solid State Chem 115 (1995) 514.
[24] L. Barbey, N. Nguyen, V. Caignaert, F. Studer, B. Raveau, J. Solid State Chem. 112 (1994) 148.
[25] J.B. Goodenough, Phys. Review 100 (1955) 564.
[26] J. Kanomori, J. Appl. Phys. 31S (1960) 14S.
[27] V. Caignert, F. Millange, B. Domengès, B. Raveau, E. Suard, Chem. Mater. 11 (1999) 930.
[28] W.L. Roth, J. Phys. Chem. Solids 25 (1964) 1.
[29] H.N. Ok, J.G. Mullen, Phys. Rev. 168 (1968) 550.
[30] R. Cacuffio, D. Rinaldi, G. Barucca, J. Mira, J. Rivas, M.A. Señarís-Rodríguez, P.G. Radaelli, D. Fiorani, J.B. Goodenough, Phys. Rev. B 59 (1999) 1068.
[31] R.D. Shannon, Acta Crystallogr. A 32 (1976) 751.